Substrate-Induced Changes in the Ammonia Channel for Imidazole Glycerol Phosphate Synthase†

Rebecca S. Myers,‡ Jordan R. Jensen,‡ Ina L. Deras,‡ Janet L. Smith,# and V. Jo Davisson*,‡

Department of Medicinal Chemistry & Molecular Pharmacology and Department of Biological Sciences, Purdue University, West Lafayette, Indiana

Received February 25, 2003; Revised Manuscript Received April 5, 2003

ABSTRACT: IGP synthase is a glutamine amidotransferase that incorporates ammonia derived from glutamine into the unusual nucleotide, N^1-[(5′-phosphoribulosyl)-formimino]-5-aminoimidazole-4-carboxamide ribonucleotide (PRFAR) to form 5′-(5-aminoimidazole-4-carboxamide) ribonucleotide (AICAR) and imidazole glycerol phosphate (IGP). A common feature of all glutamine amidotransferases is the upregulation of glutamine hydrolysis in the presence of an acceptor substrate. A refined assay system was developed to establish that *Saccharomyces cerevisae* IGP synthase shows a 4900-fold stimulation of glutaminase in the presence of the substrate acceptor PRFAR. The structure and function of IGP synthase acceptor substrate binding site were probed with competitive inhibitors that are nucleotide substrate and product analogues. In addition, these analogues were also used to establish that the normal steady-state turnover cycle involves a random sequential mechanism. Upregulation of the glutaminase active site occurs when these competitive inhibitors bind in the nucleotide site over 30 Å away. One of the key structural features of IGP synthase is that the transfer of ammonia from the glutaminase site occurs through the $(\beta/\alpha)_8$ core of the protein. Upon the basis of the recent substrate-occupied structure for yeast IGP synthase (*1*), kinetic investigations of site-directed mutants revealed that a conserved K258 residue is key to productive binding and the overall stoichiometry of the reaction. The binding of the ribulosyl phosphate portion of the substrate PRFAR appears to be transduced through reorientation of K258 resulting in a conformational switch at the base of the $(\beta/\alpha)_8$ core that enables the passage of ammonia through the core of the protein. The overall analysis also leads to further discussion of how the residues that cover the opening of the $(\beta/\alpha)_8$ in the closed state may assist the channeling of ammonia at the interface of the two functional domains in the open state.

Histidine biosynthesis is unusual as a metabolic process utilizing the purine ring of ATP as a carbon and nitrogen source (*2*). The central enzyme that forms the imidazole heterocycle and eliminates a purine metabolite is IGP synthase, a glutamine amidotransferase (GAT)[1] of the triad family (Figure 1) (*3*). A general feature of the triad GATs is the occurrence of a Cys−His−Glu triad in a glutaminase domain (or subunit) associated with acceptor domains (or subunits) featuring a variety of structural topologies (*4*). The overall efficiency of the triad GATs involves the diffusion of ammonia liberated from glutamine in one active site through a defined path or channel to an acceptor active site. As a member of the triad family of GATs, IGP synthase represents an important case of how enzymes arrive at a functional protein through adaptation of another structural motif to enable the use of glutamine as an ammonia source.

Acceptor substrate-binding activation of the glutaminase active site is a general feature of the GATs. These enzymes all have evolved mechanism(s) for transmission of the acceptor substrate binding information to the glutaminase active site (*4*). In IGP synthase, the basal glutaminase activity in the absence of an acceptor substrate is stimulated 10^3-fold in the presence of a nucleotide analogue (*3*). There are several lines of evidence that binding of the nucleotide PRFAR dictates the glutamine turnover rate. A nucleotide analogue and the product IGP are known to stimulate the catalytic properties of the glutaminase site (*5*). Also, using irreversible inhibitors of the glutamine-binding site, a previous study established that PRFAR binding leads to forward

† This work was supported by NIH Grants GM45756 (V.J.D.), DK42303 (J.L.S.), and GM24268 (J.L.S.).

* Correspondence to Department of Medicinal Chemistry & Molecular Pharmacology, Purdue University, 575 Stadium Mall Dr., West Lafayette, IN 47907-2091, 765-494-5238 (Office), 765-494-1414 (Fax), vjd@pharmacy.purdue.edu.

‡ Department of Medicinal Chemistry & Molecular Pharmacology.

Department of Biological Sciences.

[1] Abbreviations: AICAR, 5′-(5-aminoimidazole-4-carboxamide) ribonucleotide; DIPEA, diisopropylethylamine; DMPEA, dimethylphenethylamine; DMPEAA, dimethylphenethylammonium acetate; DSS, 2,2-dimethyl-2-silapentane-5-sulfonate; EDTA, ethylenediaminotetraacetic acid; HRFABMS, high-resolution fast atom bombardment mass spectrometry; O-AICAR, *N*-(hydroxyimino)-5-aminoimidazole-4-carboxamide ribonucleotide; IGP, imidazole glycerol phosphate; IGPS, imidazole glycerol phosphate synthase; PCR, polymerase chain reaction; PEP, phosphoenolpyruvate; PIPES, 1,4-piperazinediethanesulfonic acid; PRFAR, N^1-[(5′-phosphoribulosyl)-formimino]-5-aminoimidazole-4-carboxamide ribonucleotide; 5′ProFAR, N^1-[(5′-phosphoribosyl)-formimino]-5-aminoimidazole-4-carboxamide ribonucleotide; PRPP, 5-phosphoribosyl 1-pyrophosphate; RP-HPLC, analytical reversed phase high performance liquid chromatography; rPRFAR-1, N^1-[(5′-phosphoarabinitolyl)-formimino]-5-aminoimidazole-4-carboxamide ribonucleotide; rPRFAR-2, N^1-[(5′-phosphoribitolyl)-formimino]-5-aminoimidazole-4-carboxamide ribonucleotide.

10.1021/bi034314l CCC: $25.00
Published on Web 05/23/2003

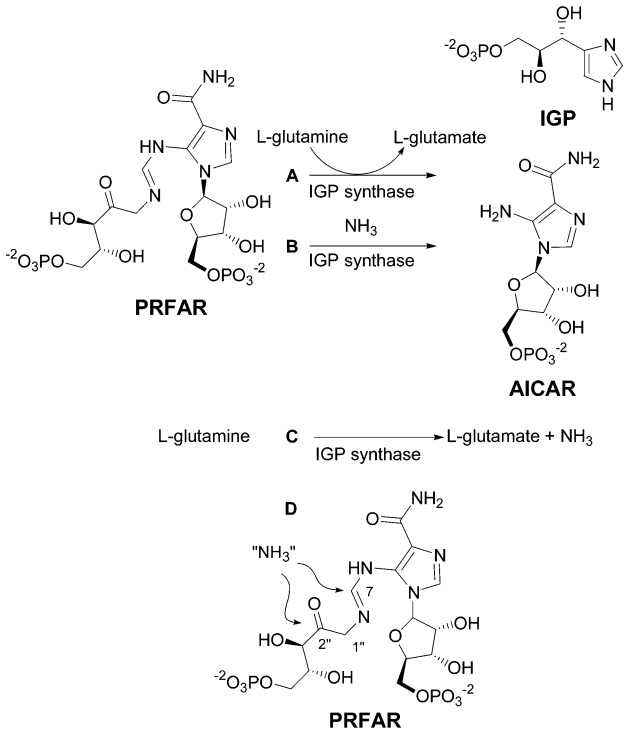

FIGURE 1: Overall reactions catalyzed by IGP synthase (HIS7). (A) Glutamine-dependent reaction. (B) Ammonia-dependent reaction. (C) Glutamine hydrolysis in the absence of PRFAR. (D) Plausible sites for ammonia attack.

commitment by addition of the active site Cys to the glutamine analogue acivicin (*6*).

The recent *Saccharomyces cerevisiae* IGP synthase structure establishes the overall distance between the nucleotide substrate (PRFAR) and glutamine binding sites as 30 Å (*7*). Importantly, the nucleotide-binding or synthase domain is a $(\beta/\alpha)_8$ barrel structural motif. The structure of the *Thermotoga maritima* enzyme verifies the general orientation of the glutaminase and synthase domains in both eukaryotic and prokaryotic IGP synthase and supports the use of the core of the barrel as part of the ammonia channel (*8*, *9*). One of the key features in these structures is the unusual cap at the bottom of the barrel. A quartet of conserved side chains with alternating charges (Arg, Glu, Lys, Glu) is observed in a conformation stabilized by electrostatic interactions that closes the bottom of the barrel core. The overall path for ammonia in IGP synthase involves transit across a domain interface region (or chamber) that lacks any significant exchange with bulk water. Modeling of the synthase domain structures with ammonia (or water) highlights how the quartet at the bottom of the barrel creates a barrier for penetration into the core. Dynamic behavior of this quartet is hypothesized to allow for the passage of ammonia at the appropriate time. In this way, the cap on the bottom of the barrel serves as an electrostatic gate that opens and closes in a coordinate fashion with the creation of ammonia in the glutaminase site. Initial evidence in support for this hypothesis is derived from the fact that an R to H mutant in the electrostatic gate of *Escherichia coli* IGP synthase isolated from a random-mutagenesis screen leads to uncoupling of the glutaminase and amidotransferase functions (*10*). In this case, the mutation resulted in a loss of ammonia due to inefficient transfer between the glutaminase and synthase sites.

An accompanying paper in this issue describes structures of the *S. cerevisiae* IGP synthase with the substrate (PRFAR) bound in the synthase site (*1*). In addition to a pair of conserved aspartate residues (D245 and D404) in the synthase domain (*11*), one other conserved residue K258 has been implicated in catalysis. There are no large global changes in the three-dimensional structure outside of the loop transition on the opening of the $(\beta/\alpha)_8$ barrel. This point is particularly true in the regions defined by the domain interface or in the regions expected to define the path of ammonia. These results indicate small changes in the side chain orientations as the primary mode for transmission of the binding event from the $(\beta/\alpha)_8$ barrel to the active site of the glutaminase.

The focus of the present study is to address in more detail the properties of the nucleotide binding site and how they impact the dynamic features of the electrostatic gate at the glutaminase−synthase interface. Nonreactive substrate analogues have been developed to explore the binding events and to probe the binding order of the substrates. Additional structure−function analyses of the basic residues in the electrostatic gate are presented that provide new insight into their functional roles in forming a path for ammonia.

MATERIALS AND METHODS

Materials. All chemicals, buffers, resins, and enzymes were purchased from commercial sources. The plasmid, p*IGPS*-T7, was prepared as previously described (*12*). PEP was synthesized according to a published procedure (*13*). Mutagenesis was performed using the QuikChange Site-Directed Mutagenesis kit from Stratagene (*14*). Custom oligonucleotides were synthesized commercially.

Diisopropylethylamine (DIPEA) was distilled from ninhydrin and stored protected from light at 4 °C. The distilled DIPEA (87 mL, 1 equiv, 0.5 mol) was added via an addition funnel over 5 h at 25 °C to a rapidly stirred solution of 29 mL of glacial acetic acid (1 equiv, 0.5 mol) and 884 mL of water to achieve pH 7.0 at the concentration of 0.5 M. (*S*)-*N*,*N*-dimethyl-1-phenethylamine ((*S*)-DMPEA) (3.3 mL) was added over 1 h at 25 °C to a rapidly stirred solution of 1.1 mL (20 mmol, 1 equiv) glacial acetic acid and 15.5 mL of water. The pH of the 0.5 M solution (1 L) was 7.0, and was stored protected from light at 4 °C.

Anion-exchange chomatography was accomplished using Q Sepharose FF resin. Cation-exchange chomatography was done with Dowex AG 50W-X8 resin. Analytical reverse-phase high performance liquid chomatography (RP-HPLC) was performed using either Microsorb-MV C-18 (4.5 × 250 mm) or PRP-1 (4.5 × 250 mm) columns. For preparative-scale RP-HPLC, either a Dynamax Macro column (22 × 300 mm) or a PRP-1 column (22 × 250 mm) was used. Mass spectrometry was performed on a ThermoQuest MAT 95 XL mass spectrometer. NMR spectrometry was performed at either 300 or 600 MHz.

N^1-[(5′-Phosphoribulosyl)-formimino]-5-aminoimidazole-4-carboxamide ribonucleotide (PRFAR). The synthesis of PRFAR was a modification of the procedure by Davisson et al. (*15*). A solution (25 mL) of 50 mM potassium phosphate, 50 mM Tris HCl, 50 mM sodium chloride, 1 mM EDTA, 10 mM ribose-5-phosphate (R5P), 12 mM ATP, and 20 mM PEP was adjusted to pH 7.6 with 5 M sodium

hydroxide. The following components were added in sequence: 16 mM $MgCl_2$, 200 U pyruvate kinase, 200 U myokinase, and 20 U PRPP synthetase. The solution was incubated at 30 °C for 45 min before addition of 25 U inorganic pyrophosphatase and 10 U HisAGIE extract. Incubation of the mixture was continued for another 2 h, and a 10 μL aliquot was assayed for PEP using lactate dehydrogenase. On the basis of the calculated amount of residual PEP present, an additional 25 U pyruvate kinase and a 1.5-fold molar excess of ADP were added, and the reaction was further incubated for 30 min. The reaction was diluted with 100 mL of cold water, filtered (0.2 μm), and applied to a 2.5 × 14 cm column of Q Sepharose FF anion-exchange resin (HCO_3^-) all executed at 4 °C. The column was washed with 60 mL of water and the compound was eluted with a gradient of NH_4HCO_3 (0−250 mM over 300 mL). The fractions eluting in the region of 250 mM NH_4HCO_3 were analyzed by UV−visible spectroscopy, and those solutions showing an A_{290}:A_{260} > 1.1, were pooled and dried by lyophilization. The resultant solid was dissolved in H_2O and eluted through Dowex AG50W-X8 (Na^+) to exchange the compound to the sodium form. Lyophilization of the eluent provided a white solid (108 mg, 65%). UV (PRFAR) λ_{max} (ϵ): 278 nm (8795 M^{-1} cm^{-1}) ^{1}H NMR (300 MHz, D_2O) δ 8.00 (1H, s, H at C2), 7.87 (1H, s, H at C7), 5.66 (1H, d, J = 5.8 Hz, H at C1′), 4.53 (1H, ψt, J = 5.7 Hz, H at C3″), 4.52 (1H, ψt, J = 5.8 Hz, H at C2′), 4.37 (1H, ψt, J = 4.8 Hz, H at C3′), 4.23 (1H, m, H at C4′), 4.11 (1H, ψq, J = 5.7 Hz, H at C4″), 4.01 (2H, m, H at C5′), 3.93 (2H, ψq, J = 5.7 Hz, H at C5″); ^{13}C NMR (90% H_2O) δ 211.5 (C2″), 170.3 (C9), 160.4 (C7), 148.3 (C5), 135.0 (C2), 120.8 (C4), 89.2 (C1′), 86.3 (d, J_{C-P} = 9 Hz, C4′), 78.3 (C3″), 76.9 (C2′), 74.2 (d, J_{C-P} = 8 Hz, C4″), 73.0 (C3′), 66.9 (d, J_{C-P} = 4 Hz, C5′), 66.8 (d, J_{C-P} = 6 Hz, C5″), 51.5 (C1″); ^{31}P NMR (D_2O) δ 3.88, 3.36; negative mode HR FABMS (glycerol) calcd 578.0901 found: 578.0925.

N^1-[(5′-Phosphoarabinitolyl)-formimino]-5-aminoimidazole-4-carboxamide ribonucleotide, Stereoisomer 1 (rPRFAR-1). One hundred fifty milligrams of PRFAR (1 equiv, 0.26 mmol) was dissolved in 50 mL of 50 mM potassium phosphate pH 7.0. To this solution was added 50 mg of $NaBH_4$, (15 equiv, 1.3 mmol) and the mixture was allowed to stir at 4 °C for 30 min. The reaction was quenched with 150 mL of water with swirling for 5 min. The crude mixture was purified by anion exchange chomatography and the two resulting diastereomers were separated by chiral ion pairing RP-HPLC (3 mM (*S*)-DMPEAA/20 mM potassium phosphate pH 7.0, 9 mL/min λ 300 nm). The first stereoisomer eluted at 27.3 min. The resulting fractions for each diastereomer were lyophilized to dryness. After freeze-drying, the residues were dissolved in 50 mL of water. (*S*)-DMPEAA and potassium phosphate was removed by anion exchange chromatography as described above. Appropriate fractions were pooled and lyophilized to dryness, producing a white solid (20 mg, 27%). The ammonium salt forms of these compounds were converted to the sodium salt by cation exchange chromatography. This material was then dissolved in 4 mL of water and stored at −80 °C. UV (rPRFAR-1) λ_{max} (ϵ): 278 nm (8795 M^{-1} cm^{-1}). ^{1}H NMR (600 MHz, D_2O) δ 7.95 (1H, s, H at C2), δ 7.89 (1H, s, H at C7), δ 5.74 (1H, d, J = 5.4 Hz, H at C1′), δ 4.58 (1H, ψt, J = 6.0 Hz, H at C2′), δ 4.40 (1H, ψt, J = 4.8 Hz, H at C3′), δ 4.26 (1H, m, H at C2″), δ 4.23 (1H, m, H at C4′), δ 3.98 (2H, m, H at C5″), δ 3.94 (2H, m, H at C5′), δ 3.81 (1H, m, H at C4″), δ 3.70 (1H, ψd, J = 9.0 Hz, H at C3″), δ 3.62 (1H, dd, J_2 = 14.4 Hz, J_3 = 7.8 Hz, H_A at C1″), δ 3.59 (1H, dd, J_2 = 13.8 Hz, J_3 = 5.4 Hz, H_B at C1″); ^{13}C NMR (150 MHz, D_2O) δ 171.0 (C9), δ 161.5 (C7), δ 149.5 (C5), δ 135.7 (C2), δ 121.4 (C4), δ 89.7 (C1′), δ 87.4 (C4′), δ 77.7 (C2′), δ 75.4 (C3′), δ 73.7 (C4″), δ 71.0 (C3″), δ 69.7 (C2″), δ 68.5 (C5″), δ 66.6 (C5′), δ 46.8 (C1″); ^{31}P NMR (300 MHz, D_2O) δ 4.45, δ 5.38; positive mode HRFABMS: calculated for $C_{15}H_{28}N_5O_{15}P_2$ 580.1057, found 580.1072.

N^1-[(5′-Phosphoribitolyl)-formimino]-5-aminoimidazole-4-carboxamide ribonucleotide, Stereoisomer 2 (rPRFAR-2). Following RPHPLC (retention time 33.6 min), the second stereoisomer was isolated from the ion-pairing reagent, (*S*)-DMPEAA and potassium phosphate by anion exchange chromatography and lyophilized to a white solid (15 mg, 20%). ^{1}H NMR (600 MHz, D_2O) δ 7.95 (1H, s, H at C2), δ 7.90 (1H, s, H at C7), δ 5.74 (1H, d, J = 5.4 Hz, H at C1′), δ 4.58 (1H, ψt, J = 6.0 Hz, H at C2′), δ 4.39 (1H, ψt, J = 4.8 Hz, H at C3′), δ 4.22 (1H, m, H at C4′), δ 4.10 (1H, m, H at C2″), δ 3.93 (4H, m, H at C5′ and C5″), δ 3.88 (1H, m, H at C4″), δ 3.81 (1H, ψt, J = 6.0 Hz, H at C3″), δ 3.74 (1H, dd, J_2 = 14.4 Hz, J_3 = 2.4 Hz, H_A at C1″), δ 3.53 (1H, dd, J_2 = 13.8 Hz, J_3 = 7.8 Hz, H_B at C1″); ^{13}C NMR (150 MHz, D_2O) δ 171.0 (C9)*, δ 161.6 (C7), δ 149.5 (C5)*, δ 135.7 (C2)*, δ 121.4 (C4)*, δ 89.6 (C1′), δ 87.4 (C4′), δ 77.7 (C2′), δ 75.7 (C3″), δ 74.7 (C4″), δ 73.7 (C3″), δ 73.2 (C2″), δ 67.9 (C5″), δ 66.5 (C5′), δ 45.6 (C1″) *values inferred from rPRFAR-1; ^{31}P NMR (300 MHz, D_2O) δ 4.42, δ 5.20 positive mode HRFABMS: calculated for $C_{15}H_{28}N_5O_{15}P_2$ 580.1057, found 580.1055.

(c) N-(Hydroxyimino)-5-aminoimidazole-4-carboxamide ribonucleotide (O-AICAR). A mixture containing 12 mM PRFAR, 200 mM potassium phosphate pH 7.0, and 120 mM hydroxylamine was stirred for 1 h at RT, filtered, and injected (1 mL) onto a preparative Hamilton PRP-1 column (22 × 250 mm) running isocractially in 25 mM DIPEAA pH 7.0/3% methanol. Hydroxyimino-AICAR eluted at 17.7 min and was observed by UV absorption at 260 nm. Peak fractions were isolated, pooled, and lyophilized to dryness. O-AICAR was converted to the sodium salt by cation exchange chomatography. Peak fractions were detected at 260 nm, pooled, lyophilized and stored at −80 °C. UV (O-AICAR) λ_{max} (ϵ): 270 nm (12 300 M^{-1} cm^{-1}). ^{1}H NMR (500 MHz, D_2O) δ 8.09 (1H, s, H at C2), δ 7.05 (1H, s, H at C7), δ 5.75 (1H, d, J = 5 Hz, H at C1′), δ 4.62 (1H, ψt, J = 5 Hz, H at C2′), δ 4.41 (1H, ψt, J = 5 Hz, H at C3′), δ 4.19 (1H, m, H at C4′), δ 3.96 (2H, m, H at C5′); ^{31}P NMR (300 MHz, D_2O) δ 4.43; positive mode HRFABMS: calculated for $C_{10}H_{17}N_5O_9P$ 382.0764, found 382.0769.

Site-Directed Mutagenesis. Oligonucleotides for site-directed mutagenesis were designed to include a restriction site to allow mutation verification by endonuclease digestion. All site-directed mutagenesis was carried out according to the protocol for the QuikChange Site-Directed Mutagenesis kit from Stratagene. Confirmatory sequencing of the plasmids was performed by the Purdue Genomics Core Facility.

Protein Purification. Purification of his-tagged IGP synthase from *S. cerevisiae* was performed as previously described (*7*) with the following modifications. Eluted fractions from the His-Bind column were diluted to a

concentration of 1.5 mg/mL in thombin cleavage buffer (20 mM Tris HCl, pH 8.4, 150 mM KCl, 2.5 mM $CaCl_2$) with 1 U/mg thombin added. The reaction was incubated at 25 °C for 5 h with constant shaking (150 rpm). Cleaved protein was isolated by His-Bind column and target fractions were pooled and concentrated using an ultrafiltration stirred pressure cell. The concentrate was dialyzed against 10 mM PIPES, pH 7.0, 5 mM EDTA.

IGP Synthase Assays. Glutamine-dependent synthase activity assays were performed as previously described (*12*). Steady-state kinetic assays of IGP synthase activity in the presence of ammonium were performed in a 96-well UV-transparent plate with a final volume of 250 μL, containing 50 mM PIPES, pH 7.0, 0.5 mM EDTA, 400 mM NH_4Cl and varying concentrations of PRFAR. Eight separate readings for each concentration were analyzed and the plates were read with a UV−Vis/fluorescence spectrophotometric plate reader.

Glutaminase Assays. Steady-state kinetic assays of the glutaminase half-reaction or stimulated glutaminase (in the presence of substrate analogues or products) were performed in a 96-well PCR reaction plate with a final volume of 100 μL, containing 50 mM PIPES, pH 7.0, 0.5 mM EDTA, 100 mM PRFAR, and glutamine (0.25−20 mM). The plate was incubated at 30 °C for 15 min with constant shaking (200 rpm), immersed in a sand bath at 125 °C for 1 min, then cooled on ice. The amount of glutamate formed was determined by the addition 50 mM Tris HCl, pH 8.0, 50 mM KCl, 1 mM EDTA, 0.5 mM 3-acetylpyridine adenine dinucleotide (APAD), and 5 μg of glutamate dehydrogenase to a final volume of 250 μL. The plate was incubated for 1.5 h at 37 °C with constant shaking (200 rpm). Transfer of 200 μL aliquots from each well to a 96-well UV-transparent plate allowed the measurement of the amount of APADH formed by absorbance changes at 363 nm ($\epsilon_{363} = 8900\ M^{-1}\ cm^{-1}$). Glutamate concentrations were determined from standard curves that were prepared in parallel on the same PCR reaction plate. Basal glutaminase activity was assayed using the same conditions as above except the IGP synthase reaction incubation time was increased to 1 h and 200 μL aliquots were transferred to a 96-well untreated black flat bottom plate. Glutamate concentrations were determined though the fluorescence of APADH (ex. 360 nm, em. 465 nm) (*16*) using standard curves prepared in parallel.

Stoichiometry Analysis. Analyses of the reaction stoichiometry catalyzed by IGP synthases were performed as previously described (*3*), with modifications: a 3 mL assay in 10 mM potassium phosphate, pH 7.5 was analyzed at various time points; 6-min intervals for 1 h, or 15-min intervals for 1.5 h.

IGP Synthase Inhibition. Inhibition assays were conducted with varying concentrations of PRFAR (2−64 μM), glutamine (0.2−49 mM), rPRFAR-1 (1−10 μM), rPRFAR-2 (1−10 μM), or albizziin (5−100 mM). Each assay (1 mL) contained 50 mM PIPES pH 7.0 and was initiated by the addition of 1 μg (16 pmol) of IGP synthase and followed at 300 nm. The extinction coefficient of 6069 $M^{-1}\ cm^{-1}$ was used for rPRFAR-1 and rPRFAR-2 based upon the similar chromophore of PRFAR. Kinetic data from these experiments were fit to models for competitive (eq 1), uncompetitive (eq 2) and mixed inhibition (eq 3).

$$v = \frac{V_{max}[S]}{K_m\left(1 + \frac{[I]}{K_{is}}\right) + [S]} \quad (1)$$

$$v = \frac{V_{max}[S]}{K_m + [S]\left(1 + \frac{[I]}{K_{ii}}\right)} \quad (2)$$

$$v = \frac{V_{max}[S]}{K_m\left(1 + \frac{[I]}{K_{is}}\right) + [S]\left(1 + \frac{[I]}{K_{ii}}\right)} \quad (3)$$

In these equations, v represents the initial velocity; V_{max}, maximal rate; [S], substrate concentration; K_m, Michealis constant; [I], inhibitor concentration; K_{is}, competitive inhibition constant and K_{ii}, uncompetitive inhibition constant (*17*).

Substrate Binding Order. Substrate competition experiments were performed over a broad range of concentrations of the two substrates. The resulting data were fit to models for ping-pong (eq 4), ordered sequential (eq 5), and random sequential (eq 6) binding:

$$v = \frac{V_{max}[A][B]}{\alpha K_A[B] + \alpha K_B[A] + [A][B]} \quad (4)$$

$$v = \frac{V_{max}[A][B]}{\alpha K_A[A] + \alpha K_B(K_A) + [A][B]} \quad (5)$$

$$v = \frac{V_{max}[A][B]}{\alpha K_A[B] + \alpha K_B[A] + \alpha K_B(K_A) + [A][B]} \quad (6)$$

where v represents the initial rate; V_{max}, maximal rate; [A], concentration of substrate A; [B], concentration of substrate B; K_A, dissociation constant for substrate A; K_B, dissociation constant for substrate B and α, the factor by which the binding of one substrate changes the dissociation constant of the other substrate.

RESULTS

Synthesis and Evaluation of Nucleotide Inhibitors. The general strategy focused on the generation and use of substrate analogues that can bind and transmit information to the glutaminase site. Although we previously established that the metabolic precursor 5′-ProFAR could mimic the substrate binding in the *E. coli* IGP synthase and stimulate the glutaminase activity, the low affinity of this compound offered limited utility (*3*). Furthermore, there remained ambiguity with regard to the substrate binding order in the two active sites of the enzyme. Together, these factors provided impetus for developing additional nucleotide inhibitors for IGP synthase.

IGP synthase catalyzes two carbon−nitrogen ligations with the nucleotide substrate PRFAR. The 2″-keto group is essential for one of the ammonia addition steps. Reduction of this group to the corresponding hydroxyl derivative using sodium borohydride afforded a pair of diastereomeric products rPRFAR-1 and rPRFAR-2 that are nonreactive substrate analogues (Figure 2). Spectral evidence for retention of the amidine group (N6−C7−N8) was initially provided

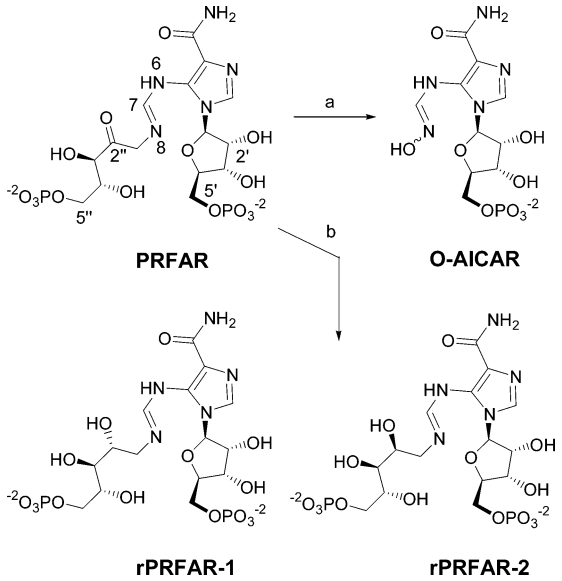

FIGURE 2: PRFAR and AICAR nucleotide analogues produced by addition reactions to PRFAR using (a) hydroxylamine or (b) $NaBH_4$.

Table 1: IGPS Steady-State Inhibition Results

substrate	inhibitor	inhibition	constants
PRFAR	rPRFAR-1	competitive	$K_{is} = 0.67 \pm 0.08\ \mu M$
PRFAR	rPRFAR-2	competitive	$K_{is} = 4.0 \pm 0.6\ \mu M$
PRFAR	albizziin	mixed	$K_{is} = 0.6 \pm 0.1$ mM
			$K_{ii} = 1.6 \pm 0.2$ mM
glutamine	albizziin	competitive	$K_{is} = 0.38 \pm 0.03$ mM
glutamine	rPRFAR-1	mixed	$K_{is} = 3 \pm 1\ \mu M$
			$K_{ii} = 1.6 \pm 0.2\ \mu M$

by the UV chromophore at 270 nm and the corresponding ^1H and ^{13}C NMR resonances. Separation of these stereoisomers required the development of a chiral ion pairing reverse phase HPLC system. As shown in Figure 2, the stereochemical assignments of each product are proposed. These assignments are based upon the comparative NMR analysis with the 1′-amino-1′-deoxyribitol and 1′-amino-1′-deoxyarabinitol (*18*). Assignments of the stereochemistry at the 2″ were based upon the relative ^1H NMR chemical shifts from C1″−C2″−C3″.

A second addition reaction with hydroxylamine was explored for product or substrate analogues. The process, which was followed by UV absorbance, provided the unique nucleotide adduct whose structure proved to be O-AICAR (Figure 2). A second product containing the ribulosyl phosphate group was recovered but not fully characterized. In previous studies with IGP synthase, evidence for the reaction product AICAR binding to the enzyme was difficult to demonstrate (*3*). O-AICAR represents a new chemical entity that has structural characteristics of both the product and the substrate.

The rPRFAR molecules and their interaction with the *S. cerevisiae* IGP synthase were evaluated by steady-state kinetic analysis. Both rPRFAR-1 and rPRFAR-2 were potent competitive inhibitors of the enzyme (Table 1). These compounds represent the first nucleotide-based inhibitors of this enzyme with the K_i for rPRFAR-1 below the K_m of PRFAR (4.6 μM). Distinctions in the binding of rPRFAR-1 and rPRFAR-2 were observed to be statistically significant despite the difference in only one stereocenter at C2″. Additionally, these compounds, as expected, were mixed inhibitors of the glutamine turnover kinetics. Complementary studies with the glutamine analogue albizziin showed that this compound is a reversible competitive inhibitor with respect to glutamine. No turnover of PRFAR is observed in the absence of glutamine, eliminating a ping-pong type mechanism. The full substrate saturation kinetic data are summarized in Table 2 and were best fit to a random sequential model, which is consistent with the inhibition data included here and those from a previous study (*6*). Together, the inhibition studies established that PRFAR and glutamine binding events are distinct and that either substrate can bind in the absence of the second substrate.

Kinetic Assays for Functional Distinctions. We utilized five different assays to assess the changes in activity caused by point mutations of the enzyme or the effect of nucleotide analogues. The overall reaction for glutamine amidotransferases can be broken down into three steps: glutamine hydrolysis, ammonia transfer, and synthesis of the product at the acceptor site (Figure 1). Glutamine hydrolysis was directly measured by quantifying the glutamate formed in the reaction. Amidotransferase activity was assessed by direct observation of the synthase reaction as PRFAR turnover at varied nucleotide substrate concentrations, in the presence of either glutamine or ammonia. The basal glutaminase activity provided an evaluation of any perturbation on the glutaminase function of the protein. Glutamate formation in the presence of PRFAR (glutaminase half-reaction) was measured to assess the nucleotide-binding signal to the glutaminase active site and functionally distinguish the glutaminase from the amidotransfer event. Most importantly, the functional consequence of perturbing any partial reaction required a careful assessment of the reaction stoichiometry to assess the efficiency of the ammonia transfer event. Therefore, the consumption of PRFAR and the formation of products AICAR and glutamate are quantitatively compared (*3*).

Modulation of Glutaminase by Synthase Products and Inhibitors. The substrate analogues, rPRFAR-1 and O-

Table 2: IGPS Steady-State Substrate Competition Results

varied substrate (A)	constant substrate (B)	binding order	constants
PRFAR	glutamine	random sequential	$\alpha K_A = 5 \pm 1\ \mu M$
			$\alpha K_B = 2.0 \pm 0.8$ mM
			$K_A = 21 \pm 15\ \mu M$
			$V_{max} = 6.0 \pm 0.3\ \mu$mol min^{-1} mg^{-1}
			$\alpha = 0.25 \pm 0.06$
glutamine	PRFAR	random sequential	$\alpha K_A = 1.7 \pm 0.4$ mM
			$\alpha K_B = 5 \pm 1\ \mu M$
			$K_A = 5 \pm 2$ mM
			$V_{max} = 5.8 \pm 0.2\ \mu$mol min^{-1} mg^{-1}
			$\alpha = 0.3 \pm 0.2$

Table 3: Stimulation of Glutaminase Activity by Products and Inhibitors

effector	K_{act}	K_m (mM)	k_{cat} (s^{-1})	k_{cat}/K_m ($M^{-1}s^{-1}$)	k_{cat}/K_m activator/basal
PRFAR	4.6 μM	1.2	6.8	5.8×10^3	4.9×10^3
rPRFAR	1.1 μM	0.9	2.15	2.3×10^3	2.0×10^3
IGP	1.4 mM	1.1	0.14	1.3×10^2	1.1×10^2
AICAR	1.3 mM	1.8	0.06	3.1×10^1	2.6×10^1
OAICAR	540 μM	0.5	0.04	8.4×10^1	7.1×10^1
IGP and AICAR		0.3	0.12	3.8×10^2	3.3×10^2
IGP and OAICAR		1.8	0.14	7.8×10^1	6.6×10^1

AICAR, and the IGPS reaction products, IGP and AICAR, were assessed for their capacity to stimulate glutamine hydrolysis (Table 3). The properties of these molecules were used as probes of the interdomain signaling because they are expected to bind within all, or part of the PRFAR (or synthase) site that is over 30 Å away from the site of glutamine hydrolysis. A modified glutaminase assay was developed that enabled a more complete analysis of the glutaminase properties. Each compound was assayed to obtain a value for K_{act} (the substrate concentration that elicits 50% of V_{max}).

In the case of normal substrate turnover with PRFAR, stimulation of glutaminase activity in the half-reaction was observed to be 4900-fold with a K_{act} consistent with the K_m for amidotransferase activity (Table 3). In the absence of an acceptor substrate, the normal products of catalysis, IGP and AICAR were able to stimulate the glutaminase activity with K_{act} at 1.4 and 1.3 mM, respectively, although 4-fold greater catalytic efficiency was achieved by IGP than by AICAR. These are consistent with the observations made with the *E. coli* IGP synthase (*3*). O-AICAR also showed similar properties with a 2.7-fold enhancement over AICAR in K_{act} indicating some binding attributes from the addition of the hydroxyimino group. As expected for a true competitive inhibitor that fills the nucleotide-binding site, the rPRFAR-1 had the lowest K_{act} at 1.06 μM consistent with the inhibitory properties observed in the normal amidotransferase turnover (Table 1). However, the overall stimulation is reduced 2.5 -fold compared to the normal substrate. Combinations of product analogues were not able to mimic the affinity and stimulation observed with the rPRFAR. There was a 3-fold synergistic effect of including both IGP and AICAR. A moderate antagonistic effect was observed when IGP and O-AICAR were combined, also consistent with the additional binding effect of the hydroxyimino group on the binding properties of O-AICAR with respect to AICAR. In this case, this group likely overlaps with the binding site occupied by IGP (*1*).

Ligand-Induced Conformations. The structure of IGP synthase in complex with PRFAR shows several protein−ligand interactions at the top of the $(\beta/\alpha)_8$ barrel (*1*). Three residues identified as interacting with PRFAR were D245, D404, and K258 (Figure 3). The impact of mutations at D245 and D404 were partially assessed in a previous study (*11*). D404 is drawn in from the inner side of the barrel opening to interact with the hydroxyls on the ribose ring of PRFAR. D245 forms part of the active site in the PRFAR−IGP synthase complex. This residue is recruited into a hydrogen bond interaction through a water bridge with the 3″-ribulosyl hydroxyl group of PRFAR and with the amine side chain of K258. Recruitment of K258 caused the greatest conformational change observed between the liganded and unliganded structures. To establish an electrostatic interaction with D474 across the PRFAR molecule, a partially disordered loop (residues 249−275) between strand fβ1 and helix fα1 moved toward PRFAR by 5−10 Å. K258 was mutated to Ala and Arg to assess its role in PRFAR catalysis and signaling.

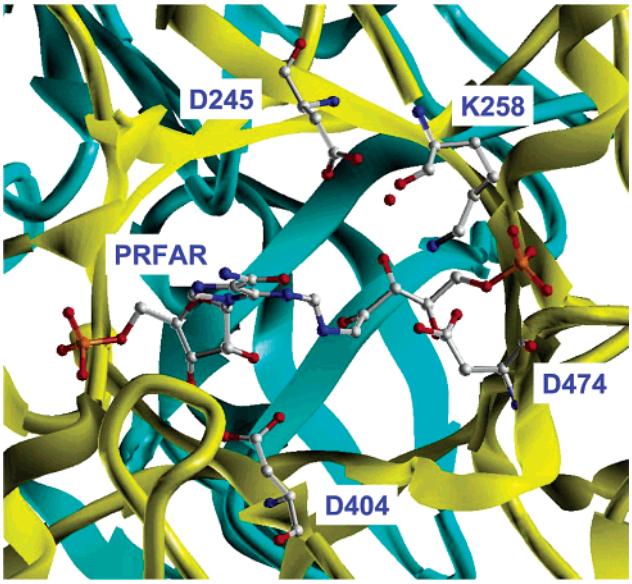

FIGURE 3: Protein−PRFAR interactions. The labeled residues are hydrogen bonded with PRFAR, either directly or via a water bridge. The glutaminase domain is blue, and the synthase domain is yellow in the ribbon diagram. Atoms of bound PRFAR and interacting residues are colored by atomic type: C white, O red, N blue, P yellow. Structure from ref *1*.

K258. Two mutations were made at this position, an Ala mutant to remove any possible hydrogen bonding interactions, and mutation to Arg to restore the positive charge of the side chain. The impact of the K258A mutation on the synthase dependent activity (Table 4) shows how critical this interaction is to maintain efficient turnover of PRFAR. From these data, it is clear the ammonia-dependent reaction mirrors the glutamine dependent reaction. However, these effects are not correlated with the glutaminase active site (Table 5) since both the basal and stimulated glutaminase functions are not altered. This differential impact of the K258A mutation on the glutaminase function and the glutamine-dependent PRFAR turnover is consistent with the uncoupling of the two active sites in IGP synthase as reflected in the overall reaction stoichiometry (Table 6). Interestingly, the relative impact of the K258A and K258R mutations are consistent with the electrostatic interaction with D474 being a key structural component for both signaling and catalysis.

Residues in the Electrostatic Gate. One part of the structural alteration upon PRFAR substrate binding is anticipated to be a conformational switch within the quartet of residues that form a barrier to the $(\beta/\alpha)_8$ core (Figure 4). A previous study using random mutagenesis showed that mutation at R239 affects the amidotransferase activity of the *E. coli* IGP synthase (*10*). The role of R239 in the coupling of the catalytic events was investigated by making three point mutations at this position including Ala, and two charged residues His and Lys. The other basic residue in the gate quartet, K360, was also mutated to Ala and Arg to assess if the two basic residues in the quartet play equivalent structural and/or dynamic roles.

Table 4: IGPS Cyclase Kinetic Parameters

mutation	K_m, PRFAR[a] (Gln) (μM)	k_{cat} (s^{-1})	k_{cat}/K_m (M^{-1} s^{-1})
wild type	5 ± 1	5.4 ± 0.5	$1.2 \pm 0.2 \times 10^6$
K258A	98 ± 7	0.045 ± 0.002	$4.6 \pm 0.4 \times 10^2$
K258R	2.0 ± 0.4	0.126 ± 0.007	$6 \pm 1 \times 10^4$
R239A	3.0 ± 0.6	$4.3 \pm 0.3 \times 10^{-3}$	$1.4 \pm 0.3 \times 10^3$
R239H	7.9 ± 0.8	$3.9 \pm 0.3 \times 10^{-2}$	$5.0 \pm 0.7 \times 10^2$
R239K	1.6 ± 0.3	$8.7 \pm 0.3 \times 10^{-3}$	$5.5 \pm 0.1 \times 10^3$
K360A	1.8 ± 0.1	0.24 ± 0.01	$1.3 \pm 0.1 \times 10^5$
K360R	2.3 ± 0.1	0.29 ± 0.01	$1.1 \pm 0.2 \times 10^5$

mutation	K_m, PRFAR[b] (NH_4^+) (μM)	k_{cat} (s^{-1})	k_{cat}/K_m (M^{-1} s^{-1})
wild type	55 ± 8	0.845 ± 0.007	$1.5 \pm 0.2 \times 10^4$
K258A	139 ± 5	$5.4 \pm 0.3 \times 10^{-3}$	$3.9 \pm 0.3 \times 10^1$
K258R	46 ± 9	$5 \pm 1 \times 10^{-3}$	$1.2 \pm 0.3 \times 10^2$
R239A	53 ± 9	0.15 ± 0.01	$2.8 \pm 0.5 \times 10^3$
R239H	75 ± 9	0.21 ± 0.02	$2.9 \pm 0.4 \times 10^3$
R239K	80 ± 6	0.30 ± 0.02	$3.8 \pm 0.3 \times 10^3$
K360A	65 ± 10	0.70 ± 0.06	$1.1 \pm 0.1 \times 10^4$
K360R	72 ± 5	0.31 ± 0.02	$4.3 \pm 0.4 \times 10^3$

mutation	K_m, Gln[c] (mM)	k_{cat} (s^{-1})	k_{cat}/K_m (M^{-1} s^{-1})
wild type	1.8 ± 0.2	6.9 ± 0.3	$3.8 \pm 0.4 \times 10^3$
K258A	6.5 ± 0.5	$2.5 \pm 0.1 \times 10^{-2}$	$3.6 \pm 0.3 \times 10^0$
K258R	1.90 ± 0.06	$15.9 \pm 0.1 \times 10^{-2}$	$8.4 \pm 0.2 \times 10^1$
R239A	6.5 ± 0.7	$6.9 \pm 0.8 \times 10^{-3}$	1.1 ± 0.2
R239H	2.1 ± 0.1	$6.0 \pm 0.1 \times 10^{-3}$	2.8 ± 0.2
R239K	1.3 ± 0.3	$9.0 \pm 0.1 \times 10^{-3}$	7 ± 1
K360A	1.96 ± 0.02	0.49 ± 0.01	$2.47 \pm 0.05 \times 10^2$
K360R	1.9 ± 0.1	1.13 ± 0.02	$5.9 \pm 0.1 \times 10^2$

[a] Reaction A in Figure 1. PRFAR was the varied substrate and the concentration of glutamine was constant at 40 mM. [b] Reaction B in Figure 1. PRFAR was the varied substrate and the concentration of NH_4^+ was constant at 400 mM. [c] Reaction A in Figure 1. Glutamine was the varied substrate and the concentration of PRFAR was constant at 100 μM.

Table 5: IGPS Glutaminase Kinetic Parameters

mutation	K_m, basal[a] (mM)	k_{cat} (s^{-1})	k_{cat}/K_m (M^{-1} s^{-1})
wild type	4.7 ± 0.2	$5.5 \pm 0.1 \times 10^{-3}$	1.18 ± 0.06
K258A	2.7 ± 0.1	$8.1 \pm 0.5 \times 10^{-3}$	3.1 ± 0.2
K258R	3.3 ± 0.1	$7.5 \pm 0.2 \times 10^{-3}$	2.3 ± 0.1
R239A	2.3 ± 0.1	$1.4 \pm 0.1 \times 10^{-3}$	0.6 ± 0.03
R239H	0.8 ± 0.1	$16 \pm 0.1 \times 10^{-4}$	2.1 ± 0.3
R239K	0.6 ± 0.5	$5.0 \pm 0.3 \times 10^{-4}$	0.8 ± 0.7
K360A	4.4 ± 0.5	$2.0 \pm 0.1 \times 10^{-3}$	0.45 ± 0.06
K360R	1.7 ± 0.2	$1.31 \pm 0.04 \times 10^{-3}$	0.7 ± 0.1

mutation	K_m, half-reaction[b] (mM)	k_{cat} (s^{-1})	k_{cat}/K_m (M^{-1} s^{-1})
wild type	1.2 ± 0.1	6.8 ± 0.2	$5.8 \pm 0.8 \times 10^3$
K258A	1.2 ± 0.1	0.172 ± 0.005	$1.4 \pm 0.1 \times 10^2$
K258R	0.64 ± 0.06	0.164 ± 0.002	$2.6 \pm 0.2 \times 10^2$
R239A	0.35 ± 0.02	0.180 ± 0.001	$5.2 \pm 0.5 \times 10^2$
R239H	1.62 ± 0.07	$0.24 \pm 0.0.02$	$1.5 \pm 0.1 \times 10^2$
R239K	1.04 ± 0.02	0.366 ± 0.009	$3.5 \pm 0.1 \times 10^2$
K360A	1.9 ± 0.3	7.8 ± 0.6	$4.1 \pm 0.8 \times 10^3$
K360R	1.24 ± 0.08	0.61 ± 0.01	$4.9 \pm 0.3 \times 10^2$

[a] Reaction C in Figure 1. Glutamine hydrolysis in the absence of PRFAR. [b] Reaction A in Figure 1. Glutamine was the varied substrate and the concentration of PRFAR was constant at 100 μM.

R239. Mutations at this position in the closure to the barrel core (Ala, His, Lys) exhibited marked decreases in the glutamine dependent PRFAR turnover (Table 4), even though R239 resides 15 Å from the synthase active site (Figure 4).

Table 6: Stoichiometry of Reaction Glutamine: PRFAR Turnover

wild type	1:1
K258A	43:1
K258R	3:1
R239A	122:1
R239H	154:1
R239K	40:1
K360A	3:1
K360R	1:1

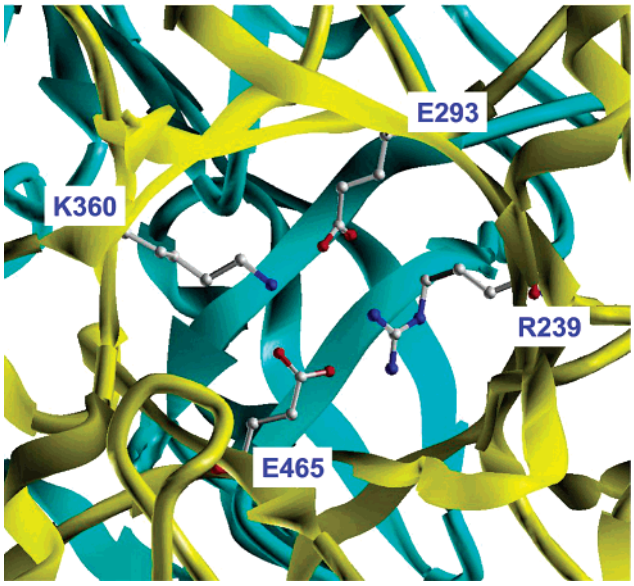

FIGURE 4: Electrostatic gate. A conserved quartet of charged residues (R239, E293, K360, E465) cap the bottom of the hydrophobic ammonia tunnel within the core of the $(\beta/\alpha)_8$ barrel and form an electrostatic gate between domains. Rendering as in Figure 3.

A 10^3 reduction in k_{cat}/K_m was observed for all three mutants in the glutamine dependent synthase reaction (Table 4); only a minimal effect for the same kinetic constants was observed in the glutaminase half-reaction (Table 5) under the same conditions. This difference in the glutamine turnover was supported by the overall stoichiometry of the reactions catalyzed by these mutant IGP synthases showing an uncoupling of glutamine and PRFAR turnover. Even in the case of the conservative mutation R239K, 40 glutamines were hydrolyzed for every synthase turnover (Table 6). These data are consistent with a proposed role of R239 in gating the entry of ammonia to the $(\beta/\alpha)_8$ core through a conformational change.

K360. A complementary basic residue in the barrier to the $(\beta/\alpha)_8$ core was mutated to Ala and Arg. For both mutants, the synthase activities were similar to wild type (Table 4). The stoichiometry of the reaction was 3:1 for K360A indicating some degree of uncoupling due to loss of ammonia. The K360R mutant also retains both structural and functional integrity of the enzyme in the case of glutaminase functions (Table 5). Most importantly, the unit stoichiometry of the reaction is retained (Table 6) demonstrating that the normal opening and closing mechanism is not compromised by the Arg mutation.

DISCUSSION

Dynamic Properties of Substrate Binding. Overall, the evolutionary process has constrained the acceptor domains

of GATs to become efficient at regulating the glutaminase domain so that ammonia can be shuttled when the acceptor substrate is present. While the glutaminase domains within the triad family are all similar, the structures of the acceptor domains indicate a wide variation in mechanistic scenarios for channeling ammonia (*19*−*25*). To date, the characterization of the molecular switches within the glutamine amidotransferases has been minimal (*20, 26*−*31*). IGP synthase offers a particularly important platform for study since the structural core is defined in the acceptor domain as the $(\beta/\alpha)_8$ barrel and presents a defined channel for ammonia. The results presented here highlight the importance of the dynamics of the residues at the interface of the glutaminase and synthase domains in regulating the production and transfer of ammonia.

A common feature among glutamine amidotransferases is the enhancement of glutamine hydrolysis in the presence of an acceptor substrate (*4*). In IGPS, a 4900-fold enhancement is measured when PRFAR occupies an active site 30 Å away from the glutamine-binding site (Table 3) with the major effect being on k_{cat} for the reaction. The additional information from the substrate binding data now corroborate the results from inhibition studies with acivicin where a 10^3-fold enhancement of k_{inact}/K_i^{app} was observed in the presence of PRFAR (*6*). In this case, the addition reaction of the active site Cys to the heterocycle in acivicin is a mechanistic corollary to the glutaminase function. There was also evidence that the inhibitor and PRFAR binding events were random with a high degree of kinetic selection for the inactivation event due to a 10^2 increase in the irreversible binding event analogous to the glutaminase reaction. The substrate competition experiments presented here indicate that the stimulation of glutaminase results in an enhancement of PRFAR turnover. The relative cellular concentrations of the two substrates are expected to be millimolar glutamine versus sub-micromolar of the labile metabolic intermediate PRFAR. Occupancy of the glutamine active site would be nearly constant (close to K_m) and enable efficient capture of the PRFAR in the synthase domain. This general feature would be expected of other enzymes in this class that require efficient flux of intermediate metabolites through key points in a pathway.

The synthase active site has several sites of protein−ligand interaction (*1*) that are required for stimulation of glutaminase by PRFAR and the analogues and products. Both IGP and AICAR partially stimulated glutaminase activity, however, IGP conferred greater catalytic efficiency than did AICAR. When administered together, there was a small synergistic enhancement of the signal. It is likely that the phosphate-binding region for AICAR plays at least some role in transmitting information. However, there is more to the binding event than phosphate recognition. For instance, the k_{cat}/K_m for glutaminase in the presence of O-AICAR was a 2.7-fold increase over that for AICAR, which indicates that the hydroxyimino group enhances binding of the AICAR moiety in the active site. However, O-AICAR in this context was mildly antagonistic when combined with IGP relative to AICAR when combined with IGP. Structural comparison of O-AICAR with the bound PRFAR leads to the proposal that the hydroxyimino group most likely binds to D404, a residue that also interacts with C-7 of PRFAR (*1*). A previous study provided additional evidence that conserved D404 is critical for catalytic function (*11*). Upon the basis of this model, the imidazole ring of IGP would also interact at this residue. When O-AICAR and IGP are both present, a competition for this overlapping region would occur. These data show that partial coverage of the active site will elicit some, but not the full, glutaminase function. For normal function, a coordinated binding event throughout the site is most likely required.

The substrate analogue rPRFAR-1 showed a high degree of substrate mimicry in the glutaminase stimulation. There is a clear correlation with the rPRFAR-1 K_{act} (substrate concentration that elicits half the maximal activity) and K_{is}, indicating the degree of glutaminase activation is directly related to binding of the substrate. These data confirm that the substrate-binding event stimulates glutaminase activity. In this case, it is assumed that the ammonia would gain access to the $(\beta/\alpha)_8$ interior but the lack of a reactive site at C2″ of rPRFAR allows the ammonia simply to leak out of the active site. The likely mechanistic consequences of the rPRFAR binding are also indicated by the (small but significant) differential inhibition observed for the two stereoisomers. From the PRFAR-bound IGP synthase structure, D245 and K258 interact with the hydroxyl group at O3″ (*1*). There is also an interaction between N469 and the carbonyl at O2″. In the phosphoarabitinoyl form of reduced PRFAR (rPRFAR-1) the hydroxyl would point toward N469 while in the phosphoribitiloyl form (rPRFAR-2), this hydrogen-bonding partner would not provide additional interaction with the enzyme.

The Role of R239. The two basic residues in the barrel closure at the domain interface, R239 and K360, have different functional roles. As displayed by the K360R mutant, only a minimal alteration in the catalytic properties was observed with no impact on the overall reaction stoichiometry. In contrast, mutations at R239 had profound effects on the kinetic properties of the synthase activity reflected in the uncoupling of the glutaminase function in IGP synthase. The alanine mutants of the two basic residues in the electrostatic gate exhibit quite different kinetic properties. K360A had little effect on the coupling of the two reactions, whereas R239A caused uncoupling such that 122 glutamine equivalents were hydrolyzed for every PRFAR. The evidence points to a dynamic, functional, "gating" role for the R239, whereas the K360 plays a structural role. The proposed distinctive roles for these residues are supported by the minimal impact of the K360R mutation on the reaction stoichiometry. There appears to be an additional role for R239 beyond the gating function. Eliminating the side chain of a member of the electrostatic quartet alters the gate and should allow ammonia to pass into the hydrophobic $(\beta/\alpha)_8$ core of the synthase domain. What is observed is a significant degree of uncoupling with R239A indicating that ammonia is likely escaping from the interdomain chamber. The function cannot be compensated by a conservative Arg or His mutation.

There is a water-filled pocket at the domain interface near R239 that can be seen in the space-filling model of IGP synthase. A highly conserved region on the glutaminase domain (P120−W124) adjacent to this pocket creates potential interdomain contacts for R239 (Figure 5). Small structural changes induced by PRFAR binding may allow

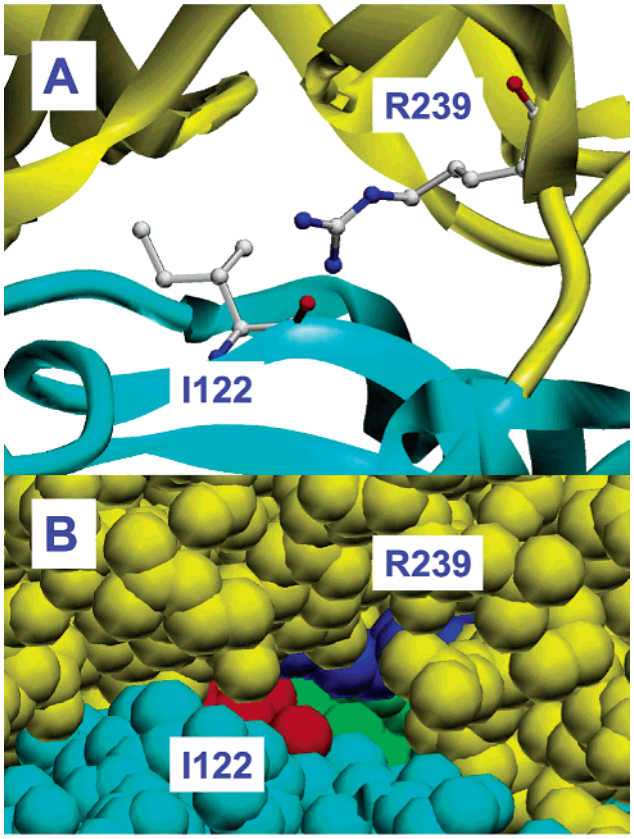

FIGURE 5: Model of gate-open position for R239. An interdomain contact between R239 and the I122 backbone carbonyl is proposed. According to the model, R239 releases from its partners in the electrostatic gate to interact with the I122 carbonyl, thus opening the gate to the hydrophobic ammonia tunnel. (A) Ball-and-stick representation of the proposed interaction of R239 side chain and I122 carbonyl. Rendering as in Figure 3. (B) Space-filling model showing the interdomain chamber near I122. R239 is in blue, I122 is in red, residues lining chamber are in green, other atoms from the glutaminase domain are in cyan, and atoms from synthase domain are in yellow. View is from the molecular exterior. Opening to the chamber is narrower than a water or ammonia molecule.

R239 to move away from its electrostatic partners into the internal pocket, which is filled by three water molecules in the crystal structure. For instance, the carbonyl of the invariant I122 is 3.5 Å from the guanidinium group of R239. Other potential hydrogen bonding partners for the side chain include the carbonyl oxygens of invariant residues T237 and the side chains of Asn233 or Asp518. Such a shift in the R239 position would, in addition to opening the gate, provide a defined path for the liberated ammonia through the center of the $(\beta/\alpha)_8$ barrel to the synthase active site. The implications are that the evolutionary process has extensively optimized the interface residues to achieve efficient ammonia transfer.

The Glutaminase Stimulus. These studies have focused on a subset of interactions that are required for opening of the electrostatic gate and the likely path that ammonia takes from one active site to the other. The high degree of glutaminase regulation by PRFAR binding is reflected in the k_{cat} for the glutaminase active site, and is not fully explained by the data presented here. For instance, the mutation R239A decreased the glutaminase half-reaction by only 11-fold over wild type, while the stoichiometry of the overall reaction was greatly disrupted. Furthermore, the substrate and product analogue studies indicate that binding in both parts of the active site is required for full glutaminase stimulation. Other protein−ligand interactions in the PRFAR active site must confer a signal directly to the glutaminase active site. There are invariant residues at the domain interface that may directly confer this signal to the glutaminase active site and are currently under investigation.

ACKNOWLEDGMENT

We thank Michelle Browne and for her technical support and Barnali N. Chaudhuri for many helpful discussions.

REFERENCES

1. Chaudhuri, B. N., Lange, S. C., Myers, R. S., Davisson, V. J., and Smith, J. L. (2003) *Biochemistry 42*, 7003−7012.
2. Alifano, P., Fani, R., Lio, P., Lazcano, A., Bazzicalupo, M., Carlomagno, M. S., and Bruni, C. B. (1996) *Microbiol. Rev. 60*, 44−69.
3. Klem, T. J., and Davisson, V. J. (1993) *Biochemistry 32*, 5177−86.
4. Zalkin, H., and Smith, J. (1998) *Adv. Enzymol. Relat. Areas Mol. Biol. 72*, 87−144.
5. Klem, T. (1996) in *The Department of Medicinal Chemistry and Molecular Pharmacology*, Purdue University, West Lafayette.
6. Chittur, S. V., Klem, T. J., Shafer, C. M., and Davisson, V. J. (2001) *Biochemistry 40*, 876−887.
7. Chaudhuri, B. N., Lange, S. C., Myers, R. S., Chittur, S. V., Davisson, V. J., and Smith, J. L. (2001) *Structure 9*, 987−997.
8. Douangamath, A., Walker, M., Beismann-Driemeyer, S., Vega-Fernandez, M. C., Sterner, R., and Wilmanns, M. (2002) *Structure 10*, 185−193.
9. Omi, R., Mizuguchi, H., Goto, M., Miyahara, I., Hayashi, H., Kagamiyama, H., and Hirotsu, K. (2002) *J. Biochem. (Tokyo) 132*, 759−765.
10. Klem, T. J., Chen, Y., and Davisson, V. J. (2001) *J. Bacteriol. 182*, 989−996.
11. Beismann-Driemeyer, S., and Sterner, R. (2001) *J. Biol. Chem. 276*, 20387−20396.
12. Chittur, S. V., Chen, Y., and Davisson, V. J. (2000) *Protein Expr. Purif. 18*, 366−377.
13. Hirschbein, B. L., Mazenod, F. P., and Whitesides, G. M. (1982) *J. Org. Chem. 47*, 3765−3766.
14. Kunkel, T. A. (1985) *Proc. Natl. Acad. Sci. U.S.A. 82*, 488−492.
15. Davisson, V. J., Deras, I. L., Hamilton, S. E., and Moore, L. L. (1994) *J. Org. Chem. 59*, 137−143.
16. Gleitz, J., Tosch, C., and Peters, T. (1996) *J. Neurosci. Methods 67*, 97−102.
17. Segel, I. H. (1975) *Enzyme Kinetics: Behavior and Analysis of Rapid Equilibrium and Steady-State Enzyme Systems*, John Wiley & Sons, New York.
18. Blanc-Muesser, M., Defaye, J., and Horton, D. (1979) *Carbohydr. Res. 68*, 175−187.
19. Teplyakov, A., Obmolova, G., Badet, B., and Badet-Denisot, M.-A. (2001) *J. Mol. Biol. 313*, 1093−1102.
20. Binda, C., Bossi, R. T., Wakatsuki, S., Arzt, S., Coda, A., Curti, B., Vanoni, M. A., and Mattevi, A. (2000) *Structure 8*, 1299−1308.
21. Larsen, T. M., Boehlein, S. K., Schuster, S. M., Richards, N. G. J., Thoden, J. B., Holden, H. M., and Rayment, I. (1999) *Biochemistry 38*, 16146−16157.
22. Knochel, T., Ivens, A., Hester, G., Gonzalez, A., Bauerle, R., Wilmanns, M., Kirschner, K., and Jansonius, J. N. (1999) *Proc. Natl. Acad. Sci. U.S.A. 96*, 9479−9484.
23. Thoden, J. B., Holden, H. M., Wesenberg, G., Raushel, F. M., and Rayment, I. (1997) *Biochemistry 36*, 6305−6316.
24. Krahn, J. M., Kim, J. H., Burns, M. R., Parry, R. J., Zalkin, H., and Smith, J. L. (1997) *Biochemistry 36*, 11061−11068.
25. Huang, X., and Raushel, F. M. (2000) *J. Biol. Chem. 275*, 26233−26240.
26. van den Heuvel, R. H. H., Ferrari, D., Bossi, R. T., Ravasio, S., Curti, B., Vanoni, M. A., Florencio, F. J., and Mattevi, A. (2002) *J. Biol. Chem. 277*, 24579−24583.

27. Bearne, S. L., Hekmat, O., and MacDonnell, J. E. (2001) *Biochem. J. 356*, 223−232.
28. Bera, A. K., Smith, J. L., and Zalkin, H. (2000) *J. Biol. Chem. 275*, 7975−7979.
29. Bera, A. K., Chen, S., Smith, J. L., and Zalkin, H. (1999) *J. Biol. Chem. 274*, 36498−36504.
30. Thoden, J. B., Huang, X., Raushel, F. M., and Holden, H. M. (2002) *J. Biol. Chem. 277*, 39722−39727.
31. Miles, B. W., Banzon, J. A., and Raushel, F. M. (1998) *Biochemistry 37*, 16773−9.

BI034314L